ISSN:2790-1688 Volume-15-(2025)

Deformation of existing metro tunnels under close and complex construction disturbances: Case study

Zhiyuan Zhang [1], Binqing Zhan [1], Xiaoxia Zhao [1,*], Zhicheng Bai [1], Shenshen Zhu [1], Xing Gao [1]

[1] China Construction Fourth Engineering Bureau Co., Ltd. Guangzhou 510000, Guangdong, China

* 19822660870@163.com

Abstract. This paper investigates deformation mechanisms of operational metro shield tunnels induced by adjacent collinear excavation through a case study of the Hangzhou Grand Convention & Exhibition Center project. A 31-month monitoring program systematically captured tunnel displacement evolution, diaphragm wall deformation, and ground response under spatially complex conditions where excavation zones intersected parallel metro tunnels. Three principal findings emerge: Phased excavation sequences govern cumulative deformation patterns, with tunnel uplift driven primarily by stress redistribution during progressive basement excavation; Interactions between adjacent excavation pits exacerbate localized displacements near tunnel intersections, underscoring the necessity for adaptive structural countermeasures; Deformation progression exhibits significant temporal dependency, with sustained collinear unloading phases contributing disproportionately to total displacements. Post-construction monitoring data confirm stabilization trends attributable to optimized zoned excavation strategies and proximity reinforcement interventions. This study provides the basic data of tunnel deformation development and a practical framework for mitigating deformation risks in urban excavation projects interfacing with metro infrastructure.

Keywords: Shield tunnel; Foundation pit; Pile; Spatiotemporal disturbances; Structural behaviors.

1. Introduction

With the continuous increase in urbanization rates, large cities are extensively constructing subways to develop underground transportation networks and alleviate urban traffic congestion. Due to land scarcity in urban areas, after subway construction and excavation are completed, the excavation of adjacent projects inevitably affects existing subway tunnels, imposing additional stress and causing significant additional deformation. In severe cases, this can lead to tunnel segment openings, segment cracking, and other structural defects in the tunnels [1, 2]. To ensure the operational safety of existing shield tunnels beneath such projects, it is critical to conduct rational analysis and reliable assessment of the deformation response of these tunnels under the influence of adjacent excavation activities [3, 4, 5].

In In recent years, a significant number of scholars have systematically investigated the deformation of underlying shield tunnels induced by foundation pit excavation through theoretical analysis [5, 6, 7], model testing [8, 9, 10], numerical simulation [11, 12], and field measurements [13, 14]. Regarding theoretical analysis, Liang et al. [6] modeled the underlying tunnel as a Timoshenko beam resting on a Pasternak foundation and, based on the two-stage method, developed a deformation solution and calculation approach, analyzing the effects of parameters such as excavation depth and foundation reaction coefficient. Chen et al. [15] conducted centrifuge model tests to study the deformation characteristics of existing underlying tunnels during foundation pit excavation, analyzing the variation laws of tunnel bulging, internal forces, earth pressure, and surface settlement, as well as the influence of excavation depth and the relative position of the foundation pit and tunnel.

In contrast to oversimplified theoretical analyses, intricate numerical simulations, and expensive model tests, on-site field measurements provide first-hand and highly reliable data, making them typically the most trustworthy source. Regarding on-site field measurements, Shen et al. [13]

investigated a foundation pit excavation project for a subway interval tunnel in Shanghai. Through field monitoring, they acquired deformation response data of the tunnel during staged foundation pit excavation. Xu et al. [14] used the deep foundation pit project of Wuhan Global Trade Center as a case study, analyzing on-site real-time monitoring data to assess its effects on a nearby subway tunnel. Zhang et al. [12] explored the impact of staged and segmented foundation pit excavation on the deformation of underlying shield tunnel structures by combining numerical simulation with analysis of on-site field measurement data.

This study presents a comprehensive analysis of a twin-basement excavation project (North Pit: 485m × 260m; South Pit: 530m × 235m) axially aligned with operational tunnels (6.2m outer diameter, 10.9–12.2m burial depth). The construction sequence, implemented over a 31-month period, directly threaten a 450-ring tunnel segment. Field monitoring data revealed time-dependent tunnel uplift patterns corresponding to staged excavation phases, with pronounced displacement observed during South Basement excavation activities at the critical 7.0m clearance zone. Post-excavation evaluations confirmed stabilized deformation parameters remained within permissible operational limits, demonstrating the technical efficacy of implemented control measures including phased construction sequencing and adjacent pile reinforcement systems.

2. Engineering Background

2.1 Tunnel, Pile, and Foundation Pit Overview

The Hangzhou Convention and Exhibition Center project includes the central corridor, the basement of the south area and the basement of the north area. The central corridor is located between the basements in the southern and northern regions, and below it is the operating Metro Line 1 tunnel. As shown in Fig. 1, the foundation pit is divided into North basement foundation pit and South basement foundation pit. The shape of the North-South foundation pit is approximately rectangular. The scale of the North foundation pit is about 485 meters from east to west and about 260 meters from south to north. The scale of south foundation pit is about 530 meters from east to west and about 235 meters from south to north. The excavation depth of foundation pit is 4.9m-7.7m.

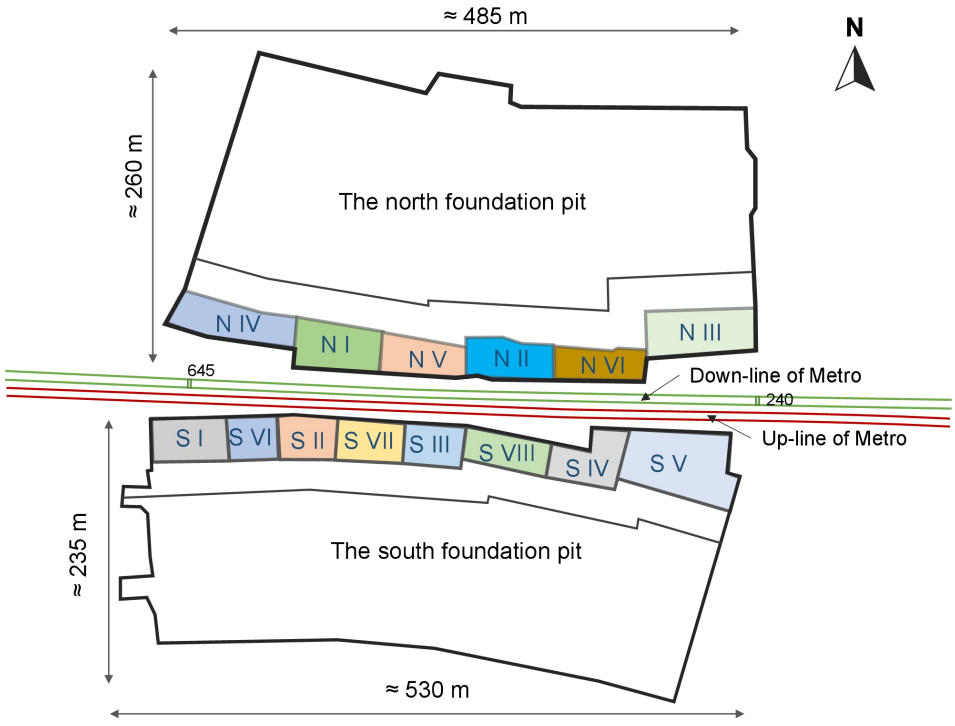

Fig. 1 Relationship between metro tunnel and foundation pit.

There is no dewatering outside the pit within 80m of the metro line. The dewatering depth beyond 80m of the metro line is 5~5.7m. The basement foundation pit near the metro line is divided into 14 independent single foundation pits (e.g., NI, NII, NIII, NIV, NV, NVI, SI, SII, SIII, SIV, SV, SVI, SVII, SVIII). The requirements for the excavation sequence of the foundation pit are important. A 1000mm diameter drilled pile (with a spacing of 1200mm) and a steel-concrete support enclosure form are used along the metro line side, combined with an 800mm TRD (Trench cutting Re-mixing Deep wall method) as a waterproof curtain.

The pile diameter of the central corridor project is 900mm, and the pile length is 75m/78m. There are 45 piles within 2.5m of the tunnel, 179 piles within 5m~10m of the tunnel, and 86 piles outside 10m of the tunnel. The nearest distance between the foundation pit supporting pile in the north area and the shield tunnel (downline) of Metro Line 1 is about 9.60m, and the nearest distance between the foundation pit supporting pile in the south area and the shield tunnel (upline) is about 7.0m. The buried depth of shield tunnel is about 10.9m~12.2m (gradually decreasing from west to East).

The outer diameter of existing shield tunnel is 6.2 meters. The inner diameter of the tunnel is 5.5 meters. The shield tunnel lining adopts assembled segments with a thickness of 0.35m. The east-west direction of the tunnel is basically parallel to the basement retaining line on the north and south sides of the project.

2.2 Geological Characteristics

Based on the excavation depth of the basement, the bottom of the basement foundation pit on the first floor of this project rests on the sandy silt of layer ①1-1 or ①1-2. The bottom of the basement foundation pit on the north and south sections, rests on the sandy silt of layer ①1-1. Within the influence range of the foundation pit of this project, the top burial depth of the shield tunnel is approximately 10.9m to 12.2m. The shield tunnel mainly passes through the ②41 sandy silt layers, and the lower soil layer of the tunnel is mainly the ③5 silt layer. The actual position of the shield tunnel and the soil layer is shown in Fig. 2.

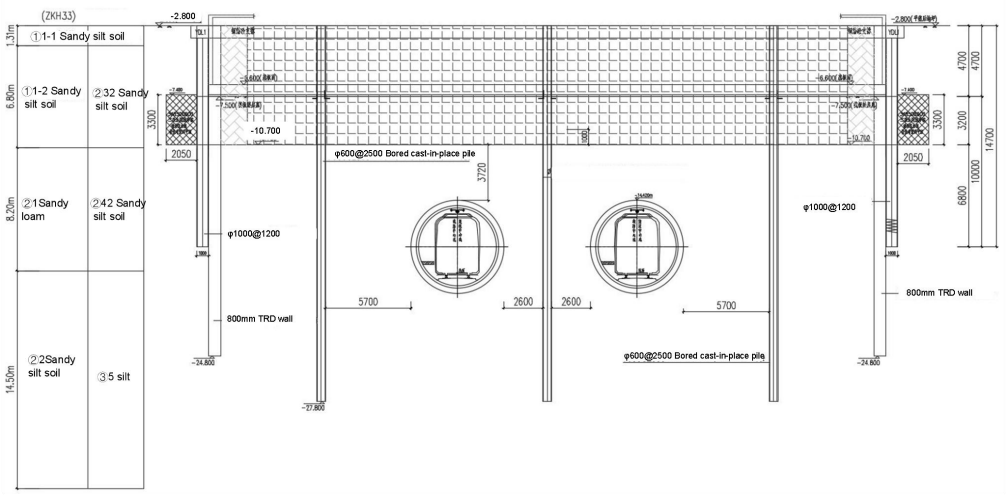

Fig. 2 Typical cross section.

2.3 Construction Process

The main process of pile construction and foundation pit is shown in Table 1. The main construction stages of the foundation pit and the construction sequence of 14 foundation pits are shown in Table 2.

Table 1. Key nodes and timeline of construction process.

Sequence	Construction stage	Time
1	Foundation pit retaining pile construction	2021.8.10~2021.11.10
2	Pile construction of central corridor	2021.11.21~2022.10.10
3	Excavation of foundation pit to completion of roof construction	2021.12.20~2022.8.15
4	Construction of foundation beam of central corridor	2022.10.20~2022.12.20
5	Superstructure construction of central corridor	~2023.05.20

Table 2. construction process of the foundation pit.

Sequence	Construction stage	Completion time
1	Support construction of S VI	2021.11.26
2	Support construction of S VIII	2021.11.26
3	Support construction of N VI	2021.11.30
4	Support construction of S VII	2021.12.1
5	Support construction of N II	2021.12.4
6	Support construction of S V	2021.12.13
7	Support construction of S III	2021.12.14
8	Support construction of N V	2021.12.21
9	Support construction of N III	2021.12.22
10	Support construction of S IV	2022.1.1
11	Support construction of S II	2022.1.4
12	Support construction of S I	2022.1.12
13	Support construction of N IV	2022.1.20
14	Support construction of N I	2022.3.11
15	Pit roof construction of N VI	2022.3.31
16	Pit roof construction of N III	2022.4.14
17	Pit roof construction of S VII	2022.4.23
18	Pit roof construction of N II	2022.5.1
19	Pit roof construction of S VIII	2022.5.2
20	Pit roof construction of S V	2022.5.7
21	Pit roof construction of S I	2022.5.24
22	Pit roof construction of N I	2022.5.24
23	Pit roof construction of N IV	2022.6.25
24	Pit roof construction of S III	2022.6.26
25	Pit roof construction of S IV	2022.7.5
26	Pit roof construction of N V	2022.7.11
27	Pit roof construction of S III	2022.7.14
28	Pit roof construction of N VI	2022.8.15

3. Performance of Existing Tunnels

The tunnel monitoring and inspection program includes the following. The monitoring contents of shield tunnels mainly include roadbed settlement, tunnel horizontal displacement, tunnel horizontal convergence, and track height difference. 102 monitoring points are set up in the tunnel, and an automated monitoring method is used to monitor the deformation data of the tunnel in real time. The tunnel appearance inspection uses manual inspection methods to check for surface defects such as cracks, water leakage, and dislocation of the tunnel segments. Cracks are measured using a crack width meter, dislocation is measured using a digital depth meter, and joint opening is measured using a feeler gauge. Tunnel segment flaw detection radar is used to detect hidden tunnel

diseases. The monitoring mainly focuses on segment rings ranging from 240 to 645 rings as shown in Fig. 1.

3.1 Tunnel Structural Defects

3.1.1 Crack and water leakage

There were 7 cases of water seepage, 10 cases of cracks, 3 cases of water streaks and 1 case of dripping in the upward tunnel (see Fig. 3). The maximum crack width of the upward tunnel was 0.08mm (at 291 rings and 399 rings), and the cumulative maximum crack width was increased by 0.08mm compared to the initial investigation stage. In the downward tunnel, there were 6 cases of water seepage, 139 cases of cracks, 2 cases of water streaks and 10 cases of dripping. The maximum crack width of the downward tunnel was 0.37mm (at 454 rings), and the cumulative maximum crack width was increased by 0.08mm compared to the initial investigation stage. The ultrasonic flaw detection of the segments showed that there were no obvious diffraction phenomena in both the upward and downward tunnels, and no obvious structural damage was found in the segments.

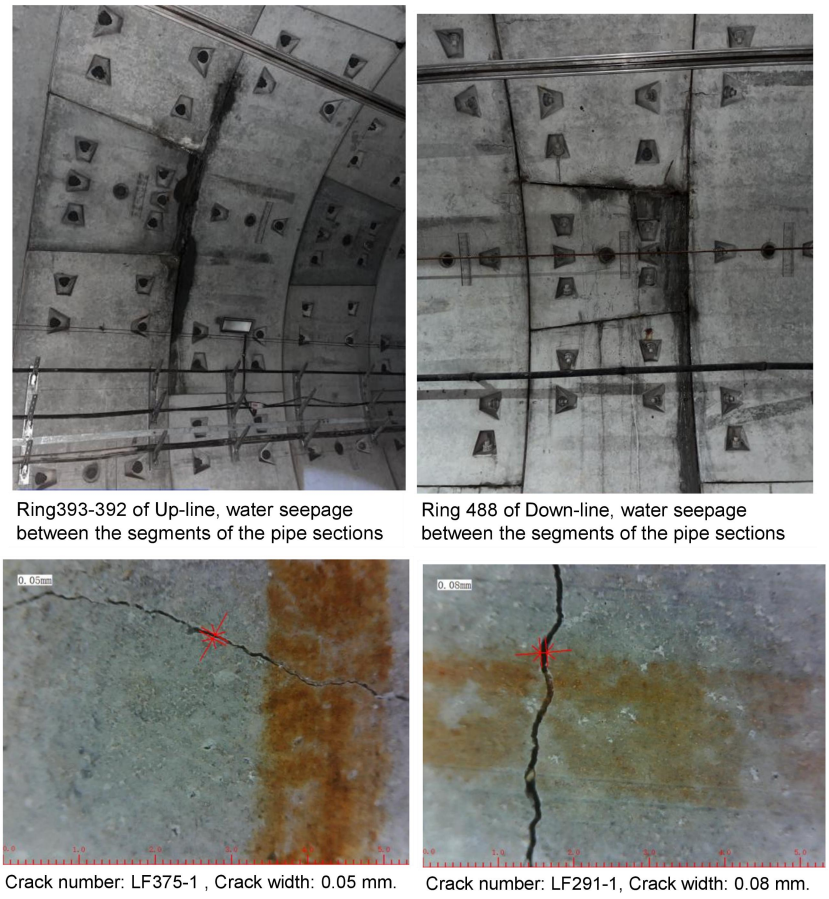

Fig. 3 Typical tunnel defect.

3.1.2 Dislocation of tunnel segments and opening of joints

According to the dislocation detection results on December 2023, the segment dislocation in the up-line tunnel were all less than 10 mm, with the maximum dislocation 6.96 mm (Ring 535 – 536). The specific dislocation distribution of up-line is shown in Fig. 4. Similarly, in the down-line tunnel, all segment dislocation remained below 10 mm, peaking at 5.76 mm (Ring 580 – 581). The majority of segment dislocation were less than 5 mm, with some instances falling between 5 mm and 10 mm.

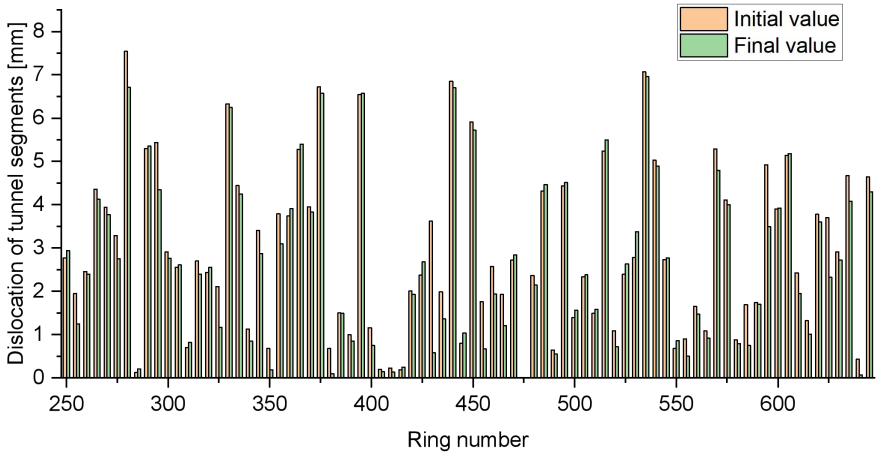

Fig. 4 Dislocation of tunnel segments in up-line (Time, March 14, 2023).

Based on the joint opening detection results from September 2023, the joint openings in the up-line tunnel segments were all under 8 mm, reaching a maximum of 5.3 mm (Ring 295–296). The down-line tunnel exhibited comparable performance, with joint openings remaining below 8 mm and a maximum opening of 5.40 mm (Ring 595–596). The joint openings were predominantly less than 5 mm, with only two exceptions (one ring in each of the up-line and down-line) measuring between 5 mm and 10 mm.

3.2 Deformation Evolution of Existing Tunnels

It is evident that throughout the implementation of this project, locations where tunnel deformation exceeded control values were primarily distributed across three nodal positions, as shown in Fig. 5. Therefore, the assessment focused on analyzing and summarizing data from these locations. Considering the construction control requirements of the central corridor, this study takes Node I (No. 585 ring to No. 630 ring) and Node II (No. 485 ring to No. 525 ring) as example to analyze the time-history curves of tunnel ballast bed settlement, and horizontal convergence throughout the project implementation. Notably, the scope of Node I covers segment rings 585 to 630 in both the upward and downward tunnel lines. The scope of Node II covers segment rings 485 to 525. The corresponding construction stages of Node I and Node II are shown in Table 3 and Table 4, respectively.

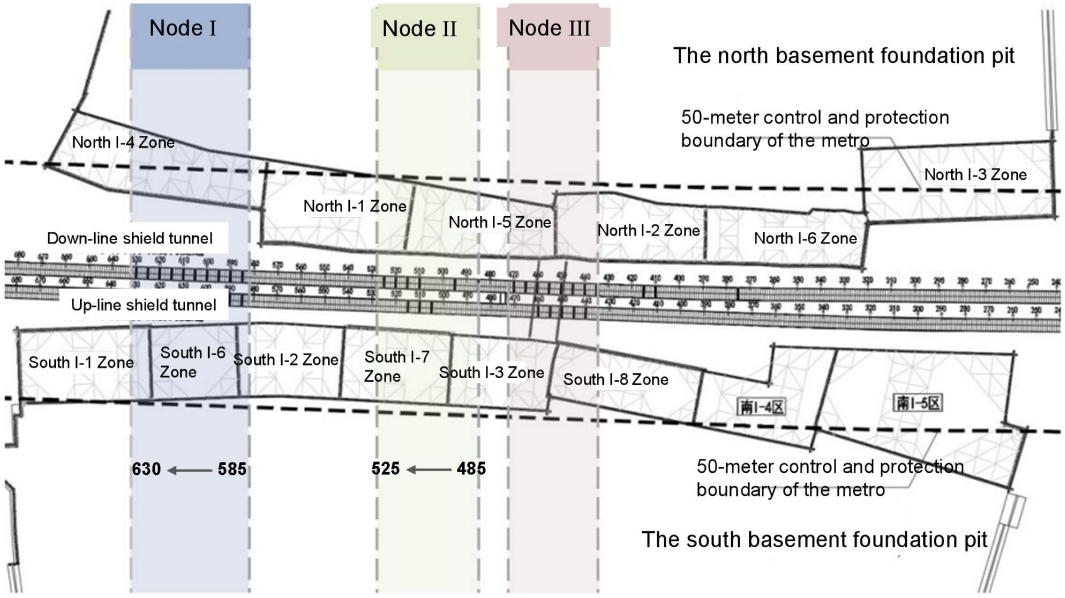

Fig. 5 Node Distribution of deformation exceeding the control threshold.

Table 3. Node I construction stage.

Sequence	Construction stage	Time
1	Foundation pit retaining pile construction	2021.8.10~2021.11.10
2	Pile construction of central corridor	2021.11.21~2021.12.30
3	Excavation of foundation pit in South VI area to completion of roof construction	2021.12.20~2022.3.30
4	Excavation of foundation pit in North IV area to completion of roof construction	2022.2.20~2022.6.25
5	Construction of foundation beam of central corridor	2022.10.20~2022.12.20
6	Superstructure construction of central corridor	~2023.05.20

Table 4. Node II construction stage.

Sequence	Construction stage	Time
1	Foundation pit retaining pile construction	2021.8.10~2021.11.10
2	Pile construction of central corridor	2021.11.21~2021.12.30
3	Excavation of foundation pit in SouthVII area to completion of roof construction	2022.01.10～2022.6.26
4	Excavation of foundation pit in South III area to completion of roof construction	2022.2.20～2022.4.23
5	Excavation of foundation pit in North I area to completion of roof construction	2022.4.20~2022.6.25
6	Excavation of foundation pit in North IV area to completion of roof construction	2022.02.20~2022.7.11
7	Construction of foundation beam of central corridor	2022.8.10~2022.11.10
8	Superstructure construction of central corridor	~ 2023.06.20

3.2.1 Convergence deformation of tunnel section

According to the full section 3D laser scanning of shield tunnel in January 2024, the convergence values of tunnel cross-sections have shown significant increases compared to the initial investigation phase across extensive sections. Notably, the convergence variation in the down-line tunnel sections generally exceeds that observed in the up-line sections. The scanning results indicate that the up-line tunnel convergence has increased by 2.8 mm to 23.7 mm relative to the initial investigation period. While the down-line tunnel convergence demonstrates a more pronounced increase ranging from 7.3 mm to 36.4 mm.

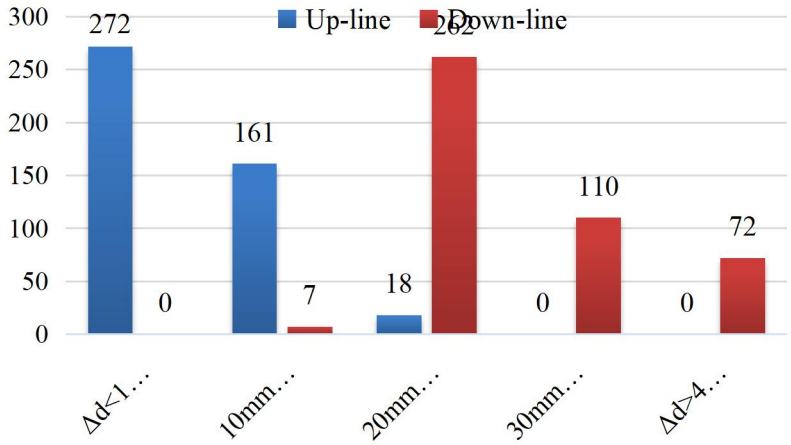

Fig. 6 Tunnel convergence distribution.

In the tunnel segments spanning rings 645 to 195, statistical analysis reveals that 451 rings in the up-line and 269 rings in the down-line exhibited horizontal convergence values of $\Delta d < 30$ mm, as present in Fig. 6. The down-line sections displayed more severe convergence characteristics: 177 rings fell within the 30 mm $\leqslant \Delta d < 55$ mm range, while 5 rings showed convergence values between 55 mm $\leqslant \Delta d < 60$ mm. The maximum convergence value in the up-line was recorded at ring No. 451, measuring 24.1 mm. Particularly noteworthy is that 182 rings in the down-line exceeded the 30 mm convergence threshold, with the maximum value reaching 55.9 mm at ring No. 448.

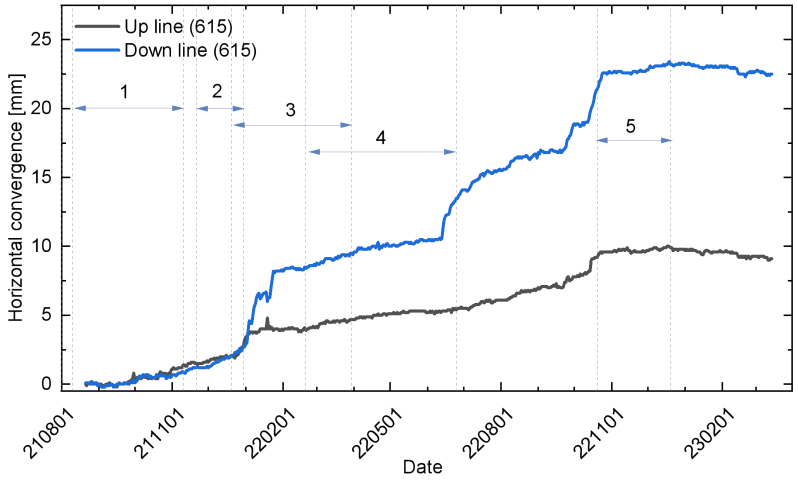

Fig. 7 Time-history curve of horizontal convergence of the tunnel within the range of Node I (ring number 615, construction stage can refer to Table 3).

The time history curve of the cumulative value of horizontal convergence of a typical section tunnel is shown in Fig. 7 (No. 615 ring of node I). Obviously, the convergence of the down line is significantly greater than that of the up line. The first stage of foundation pit retaining pile construction has little impact on tunnel convergence. The third stage of excavation of foundation pit in South VI has a significant impact on tunnel convergence.

3.2.2 Ballast bed settlement

According to long-term monitoring data in Fig. 8, the maximum cumulative settlement of the upline tunnel was -6.50mm (located at Ring 485, on March 14, 2023). Among them, there is a large settlement from ring 485 to ring 525 and ring 600 to ring 645.

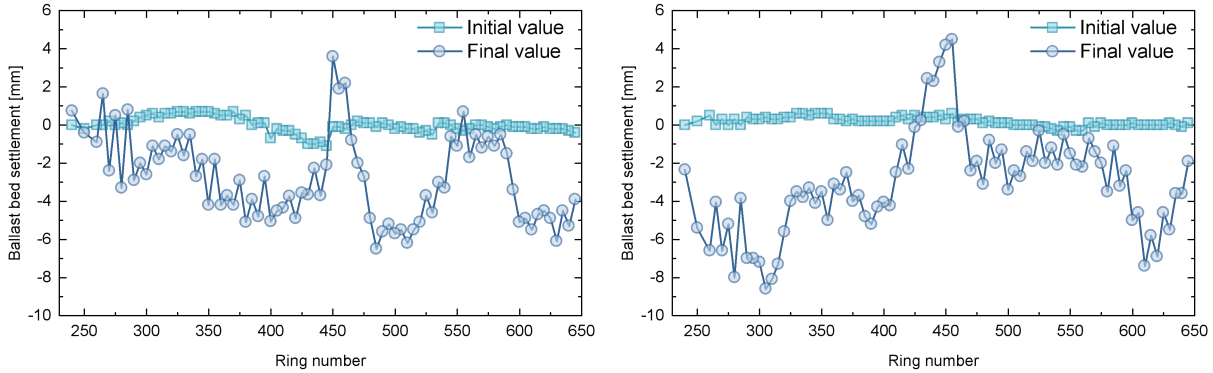

(a) Up-line (b) Down-line

Fig. 8 Settlement curve of tunnel ballast bed (Time, March 14, 2023).

To analyze the main factors of settlement, the time history curve of the cumulative settlement of a typical section tunnel is shown Fig. 9 (No. 615 ring of Node I, No. 500 ring of Node II). For the No. 615 ring, the settlement trend of the up and down tunnels is consistent as presented in Fig. 9 (a).

The construction process of the South VI foundation pit and North IV foundation pit caused significant settlement of the tunnel.

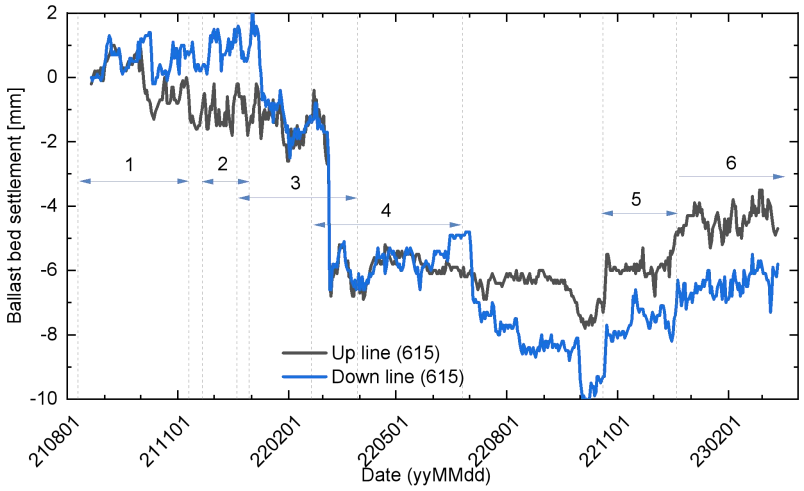

(a) No. 615 ring of Node I (construction stage can refer to Table 3).

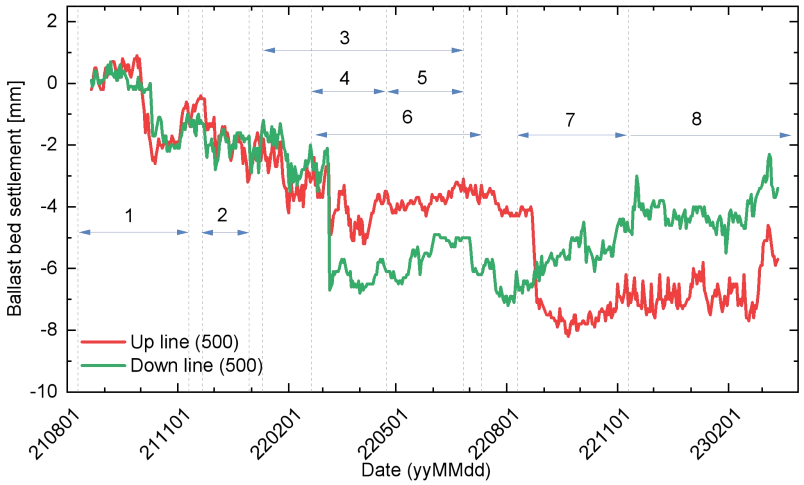

(b) No. 500 ring of Node II (construction stage can refer to Table 4).

Fig. 9 Time-history curve of tunnel ballast bed settlement.

3.3 Reasons for Exceeding Preset Control Standards

The reasons for exceeding preset control standards are analyzed as follows: i) During the construction of central corridor engineering piles, excessive construction speed and improper control of staggered construction spacing were observed. Based on field monitoring data and the spatial distribution of tunnel over-control locations, it was concluded that the intensive engineering pile construction within a short duration constituted the primary cause of excessive deformation exceeding control values in adjacent shield tunnels. ii) Despite the implementation of TRD waterproof curtains, prolonged large-scale dewatering in the extensive foundation pit caused groundwater level reduction near tunnel sections. This resulted in approximately 15-30 mm of soil layer compression due to increased additional stress, leading to measurable tunnel settlement. iii) Inadequate control of construction loads in the central corridor area, combined with intensive construction machinery operations, induced adverse effects on underlying shield tunnels.

4. Summary

This study presents a comprehensive analysis of axially aligned excavation activities for the pile and foundation pit, conducted over a 31-month monitoring Metro Line 1 shield tunnels in soft soil deposits. Systematic evaluation of tunnel deformation yielded the following principal finding:

(1) Tunnel structures demonstrated predominant vertical deformation during staged excavation, attributable to stress redistribution from phased basement excavation. Displacement magnitudes showed significant temporal correlation with excavation duration, while constrained convergence deformation reflected the effectiveness of structural reinforcement countermeasures.

(2) Extended axially aligned excavation operations induced stress superposition effects, particularly through pit-corridor-pit interactions, which significantly amplified tunnel settlement and deformation. This spatiotemporal coupling mechanism was identified as the primary contributor to observed deformation progression.

(3) The intensive engineering pile construction within a short duration constituted the primary cause of excessive deformation exceeding control values in adjacent shield tunnels. The division of engineering piles and foundation pits, as well as the sequence of their construction, still deserve further optimization to reduce the impact on tunnels.

The comprehensive construction documentation and deformation monitoring datasets provide critical benchmarks for urban excavation projects overlying active metro infrastructure. Subsequent investigations should combine numerical simulations with empirical observations to elucidate the fundamental mechanisms governing time-dependent deformation under axially aligned excavation scenarios.

References

[1] Huang, H., Shao, H., Zhang, D., et al. Deformational responses of operated shield tunnel to extreme surcharge: a case study. Structure and Infrastructure Engineering, 2017, 13(3): 345-360.

[2] Chen, R., Meng, F., Li, Z., et al. Investigation of response of metro tunnels due to adjacent large excavation and protective measures in soft soils. Tunnelling and Underground Space Technology, 2016, 58: 224-235.

[3] Zhao, Y., Gong, Q., Tian, Z., Zhou, S., & Jiang, H. (2019). Torque fluctuation analysis and penetration prediction of EPB TBM in rock–soil interface mixed ground. Tunnelling and Underground Space Technology, 91, 103002.

[4] Liu, B., Yu, Z., Hang, Y., et al. A simplified combined analytical method for evaluating the effect of deep surface excavations on the shield metro tunnels. Geomechanics and Engineering, 2020, 23(5): 405-418.

[5] Cheng, K., Xu, R., Ying, H., et al. Simplified method for evaluating deformation responses of existing tunnels due to overlying basement excavation. Chinese Journal of Rock Mechanics and Engineering, 2020, 39(3): 637-648.

[6] Liang, Z., Tang, D., Huang, M., et al. Simplified analytical method for evaluating the effects of adjacent excavation on shield tunnel considering the shearing effect. Computers and Geotechnics, 2017, 81: 167-187.

[7] Zhou, S. H., Guo, P., & Stolle, D. F. (2018). Interaction model for “shelled particles” and small-strain modulus of granular materials. Journal of Applied Mechanics, 85(10), 101001.

[8] Zhang, Y., Xie, Y., Weng, M. Centrifugal test on influence of asymmetric foundation excavation to an underlying subway tunnel. Rock and Soil Mechanics, 2018, 39(7): 2555-2562.

[9] Zhou, S., Jiang, H., Fu, L., Shan, Y., Ye, W., & Guo, P. (2023). Experimental study on deformation and strength characteristics of granular soil-structure interface under coupled monotonic shear and vibration using a modified direct shear apparatus. Acta Geotechnica, 18(6), 2899-2913.

[10] Wu, Y., Zhao, Y., Gong, Q. et al. Alternant active and passive trapdoor problem: from experimental investigation to mathematical modeling. Acta Geotech 2022; 17, 2971–2994.

[11] Huan, X., Shi, L., Jin, L., et al. Effect of divided excavation of long and narrow foundation pits on existing shield tunnels in soft soil area. Journal of Zhejiang University of Technology, 2020, 48(3): 261-268.

[12] Zhang, Z., Xi, X., Wu, L. Numerical simulation and site monitoring analysis of influence of division excavation of foundation pit on adjacent large-diameter river-crossing tunnel. Tunnel Construction, 2018, 38(09): 1480-1488.

[13] Shen, W., Shen, R., Sun, L. Field monitoring and analysis on the influence of deep excavation on adjacent metro. Chinese Journal of Underground Space and Engineering, 2019, 15(Suppl.1): 354-360.

[14] Xu, S., Zhou, Q., Zheng, W., et al. Influences of construction of foundation pits on deformation of adjacent operating tunnels in whole process based on monitoring data. Chinese Journal of Geotechnical Engineering, 2021, 43(5): 804-812.

[15] Chen, R., Al-madhagi, A., Meng, F. Three-dimensional centrifuge modeling of influence of nearby excavations on existing tunnels and effects of cut-off walls. Chinese Journal of Geotechnical Engineering , 2018, 40: 6-11.